Delamination toughening of composite laminates using weakening or toughening interlaminar patches to initiate multiple delaminations

A numerical study

Trabal, Guillem Gall; Bak, Brian Lau Verndal; Chen, Boyang; Jensen, Simon Mosbjerg; Lindgaard, Esben

DOI
10.1016/j.engfracmech.2022.108730

Publication date
2022

Document Version
Final published version

Published in
Engineering Fracture Mechanics

Citation (APA)
Trabal, G. G., Bak, B. L. V., Chen, B., Jensen, S. M., & Lindgaard, E. (2022). Delamination toughening of composite laminates using weakening or toughening interlaminar patches to initiate multiple delaminations: A numerical study. *Engineering Fracture Mechanics*, *273*, Article 108730. https://doi.org/10.1016/j.engfracmech.2022.108730

Engineering Fracture Mechanics 273 (2022) 108730

Contents lists available at ScienceDirect

Engineering Fracture Mechanics

journal homepage: www.elsevier.com/locate/engfracmech

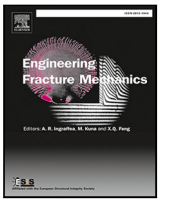

Delamination toughening of composite laminates using weakening or toughening interlaminar patches to initiate multiple delaminations: A numerical study

Guillem Gall Trabal [a], Brian Lau Verndal Bak [a], Boyang Chen [b], Simon Mosbjerg Jensen [a], Esben Lindgaard [a,*]

[a] CraCS Research Group (cracs.aau.dk), Department of Materials and Production, Aalborg University, Fibigerstraede 16, DK-9220, Aalborg East, Denmark

[b] Faculty of Aerospace Engineering, Delft University of Technology, Kluyverweg 1, 2629 HS Delft, Netherlands

ARTICLE INFO

Keywords:
Multiple delaminations
Delamination toughening
Floating Node Method
Adaptive refinement
Cohesive Zone Modelling

ABSTRACT

A numerical study on toughening laminated composite materials against delamination by initiating multiple interlaminar cracks is presented. Different configurations of interface toughening and weakening patches, that modify the interface properties at selected locations, are investigated as a way to trigger multiple delaminations. Both interface toughening and weakening patches can be configured to toughen the laminated material by initiating multiple delaminations. The initiation of multiple delaminations and the increase in toughness depend on the interface strengths and toughness of the patches. The main mechanisms behind the initiation of multiple delaminations for both cases are presented. An adaptive refinement method implemented within a Matlab Finite Element Analysis code that models the interfaces of the laminate with cohesive elements is used for the analyses. The adaptive refinement framework allows efficient analysis of multiple delaminations with very fine meshes at the wake of the crack tips. A discussion on the overall performance of the toughening concept, and the main parameters affecting the results, i.e. the length of the interface toughening or weakening patches, the distance of the substrate between the affected interfaces, and the material's mechanical properties, is carried out. The results presented in the paper show that a toughening effect against delamination can be achieved using interface toughening or weakening patches to onset multiple delaminations.

1. Introduction

Delamination is the separation of the layers in a laminated fibre reinforced polymer (FRP) and constitutes one of the main damage modes leading to the final failure of a composite structure. Delamination is initiated by e.g. intralaminar damage, geometric details, manufacturing defects or out-of-plane loading, and propagates in the interface between the laminate's layers [1–4]. Delamination cracks may propagate under quasi-static and fatigue loading conditions [5–8], and can be difficult to detect and address once the structure is in use [9]. Therefore, it is important to avoid the initiation and propagation of such cracks.

Several methodologies have been proposed in the literature to toughen interfaces against delamination or to avoid its initiation. In [10,11] it is proposed to change the lay-up stacking sequence to reduce inter-laminar stresses, which in turn reduces the likelihood

* Corresponding author.
E-mail addresses: ggt@mp.aau.dk (G.G. Trabal), brianbak@mp.aau.dk (B.L.V. Bak), B.Chen-2@tudelft.nl (B. Chen), smj@mp.aau.dk (S.M. Jensen), elo@mp.aau.dk (E. Lindgaard).

https://doi.org/10.1016/j.engfracmech.2022.108730
Received 15 May 2022; Received in revised form 14 August 2022; Accepted 15 August 2022
Available online 22 August 2022

of delamination initiation and propagation. Fibre bridging is also known to toughen the interface against delamination as shown in [12–15]. Moreover, delamination is driven at the micro-mechanical scale by matrix fracture and fibre–matrix detachment, which means that modifications of the constituent materials of the laminate, i.e. fibre or matrix, can result in a tougher interface. Both a tougher matrix [16–22], or an improved matrix–fibre interface [23–30] can toughen the interface. However, modifying the matrix can affect the wetting and infusion properties, while modification of the fibres may reduce the in-plane mechanical properties of the laminate. In addition, improvement of the matrix–fibre interface may induce premature failure of bridging fibres, thus reducing the fibre bridging toughening effect [31]. An approach based on engineering thin-plies of fabric with laser micro-cuts, have shown improved in-plane and interlaminar fracture toughness [32,33]. Multiscale composites that combine fibres at the nano and macro scale levels [34] have been proposed to obtain tougher matrices [35–41] by the inclusion of nanoparticles or nanofibres. Finally, adding a thin layer of nanoscale fibres fabric between layers, a technique called interleaving, has been recently used with an increase in toughness and strength but at a high economic cost [42–44]. Interface toughening is also achieved through thickness reinforcement methods such as stitching laminae together [45–48], z-pinning [49–52], 3D woven fabrics [53–55], or interlocking mechanisms [56]. Although a considerable increase in interface toughness and strength is achieved through thickness reinforcement methods, a considerable degradation in the in-plane properties is also observed [45,51]. Finally, interface toughening can be achieved by interleaving a thin polymeric based layer between the layers in a laminate, which results in an increase in toughness and strength without changing the in-plane properties [57–69]. However, using them at the structural scale in all the interfaces susceptible to damage is currently economically unfeasible.

Recent research presented in [70–72] explore the possibility of toughening the structure against delamination by purposely initiating multiple delaminations in the structure. More energy can be dissipated by increasing the area of the newly formed crack surfaces achieving a toughening effect. In [70] a combined numerical–analytical study is presented on a moment loaded DCB specimen with a weakened interface that successfully achieves multiple delaminations. A gain factor ranging between 1.2 and 1.9 in the energy release rate G calculated using the J-integral is obtained depending on the thickness of the substrate between the delaminating interfaces. The same observations have been made in [73], where tailored defects are placed at a secondary interface of the laminate. Similarly, while studying laser patterning toughening of post-cured adhesive bonding of laminates, [74] observes that bridging adhesive ligaments between the joined laminates increase the toughening effect of their bonding approach greatly. This effect is thoroughly studied in [75] where the source of the bridging ligaments is identified to be the variability of the interface toughening provided by the laser patterning. A strategy of alternating patches of pattern-toughened and pristine laminated interface is proposed in [76] to control the creation and location of the bridging ligaments.

In this work, a numerical study is performed on the promotion of multiple delaminations and its toughening effects on laminates using the ideas from [74–76]. A DCB specimen under displacement control featuring a main interface with a pre-crack and a secondary undamaged interface is used. The interfaces are modelled with a Cohesive Zone Model (CZM) from [77,78] and the adaptive refinement formulation presented in [79], with some modifications, is employed. Two different approaches are considered. Firstly, the approach followed by [70–72] is explored with the inclusion of interface weakening patches in a secondary interface of the DCB. Remark, a patch of finite length with weakened interface material properties is modelled, instead of a fully weakened plane. Secondly, the initiation of multiple delaminations by placing interface toughening patches is studied using a model with an interface toughening patch placed at the main interface of the DCB. The interface weakening and toughening patches are modelled as areas in the interface with reduced or augmented onset strength and critical energy release rate. The objectives of the presented studies are, firstly, to assess the feasibility of promoting multiple delaminations with interface toughening/weakening patches in the laminate. Secondly, to provide a detailed qualitative study of the multiple delamination initiation and subsequent propagation of the newly created delamination crack tips for the interface weakening and toughening patch cases.

The manuscript is organized as follows. Section 2 briefly outlines the method from [79] and the modifications done to model delamination onset. Section 3 presents the numerical testing protocol detailing the specimen, material and mesh used in the different numerical tests. The results of such tests are detailed in Section 4 while Section 5 discusses the findings of the presented work. Concluding remarks are done in Section 6.

2. Methods

The analyses in this work are conducted using the adaptive refinement method presented in [79] implemented in a Matlab FEA code, which offers some key advantages. Firstly, [79] features an efficient adaptive mesh refinement using a floating node method suitable for numerical studies with a high number of analyses. Secondly, the in-house code implementation in Matlab offers the required flexibility to quickly set up a large number of analyses and gather all the necessary data for the post-processing of the results. Crack initiation capabilities are developed and added to the adaptive refinement method from [79] as such feature is needed in this study to simulate initiation of multiple delaminations. This section briefly outlines the adaptive refinement method, the particular modifications that allow the initiation of new delaminations, and the underlying FE formulations for completeness and reproducibility of the results. Remark, that in this work, a cohesive interface is referred to as any interface that is discretized with cohesive elements and therefore, susceptible to undergo delamination.

The method presented in [79] is capable of adaptively refining the structure by combining the Adaptive Refinement Scheme (ARS) and the Adaptive Floating Node Method (A-FNM) element. The A-FNM element can refine and coarsen itself while including new cohesive interfaces discretized with cohesive elements (CEs). The specimen is meshed with a single A-FNM element through the thickness which, in the presented studies, can contain two cohesive interfaces as shown in Fig. 1a. During the analysis, the ARS assigns each A-FNM element interface an interface state that depends on the interface cohesive damage variable d. The available

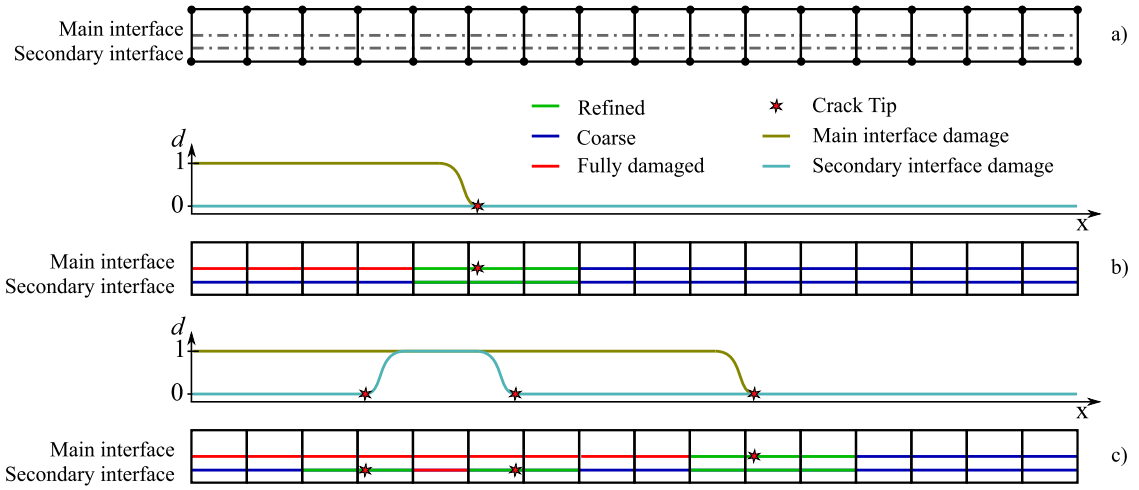

Fig. 1. Adaptive Floating Node Method (A-FNM) element interface states of the specimen shown in (a), after applying the Adaptive Refinement Scheme (ARS) for a single delamination (b), and after initiation of multiple delaminations (c).

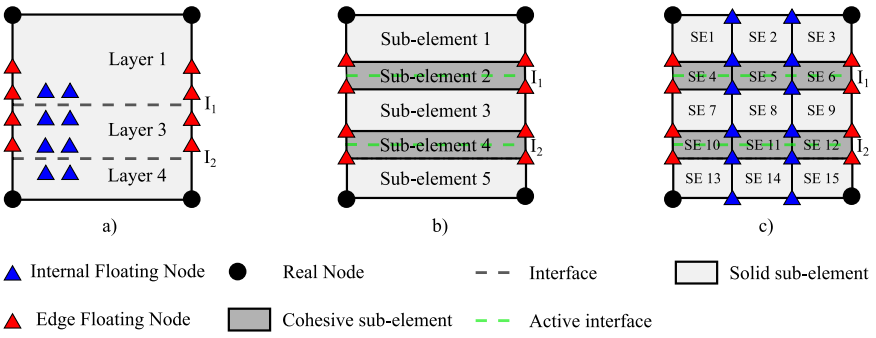

Fig. 2. Partitions on the A-FNM element triggered in this work analyses'.

interface states are (1) Fully damaged, (2) Refined, or (3) Coarse, as shown in Fig. 1b and c. Subsequently, the A-FNM element is refined or coarsened, depending on the A-FNM element interfaces states, creating several Sub-Elements (SEs) as shown in Fig. 2. This ensures a correct discretization of all the interfaces in the model, and thus providing accurate results with low computational cost. Modifications are only necessary in the ARS to model the initiation of new delaminations.

Preallocation of cohesive elements at any pristine interface has been added in contrast to [79], where cohesive elements were only inserted in the vicinity of a crack front. The ARS is applied, including the aforementioned modification, at each iteration of the Newton–Raphson solver as detailed in [79]. In this way, the ARS naturally refines the cohesive interfaces in the A-FNM element where damage may be initiated. For instance, in the early stages of the analysis in Fig. 1b, the cohesive interfaces are refined in the A-FNM elements adjacent to the A-FNM element that includes the crack tip. The fine discretization accurately allows the eventual initiation of damage, creating multiple new crack tips as seen in Fig. 1c. In this way, the ARS algorithm keeps refining the area around the crack tips following the logic outlined in [79].

The relevant configurations that the generic A-FNM element (Fig. 2a) will undertake in the studies of the current work are exemplified in Fig. 2b and c. Note, that the element can be refined further in the horizontal direction creating more SEs. The A-FNM element stiffness matrix is assembled after activation of the floating nodes [79] from the different SEs' stiffness contributions calculated using standard FE formulations. Solid SEs use the 2D linear plane strain Enhanced Assumed Strains (EAS) equivalent single layer 4-node element, named EAS4 and detailed in [79], which corrects the shear-locking in bending dominated situations featuring coarse discretizations. Cohesive SEs are formulated as 4-node zero thickness cohesive SEs following the formulation from [77,78] for analysis of delamination initiation and growth under mixed-mode loading conditions. The bilinear cohesive law shown in Fig. 3 is used.

3. Numerical testing protocol

Two sets of numerical tests have been devised featuring a single interface toughening or weakening patch using the specimen shown in Fig. 4. Both mode I and mode II critical energy release rates G_c, or onset tractions, τ_0, are scaled equally compared to the

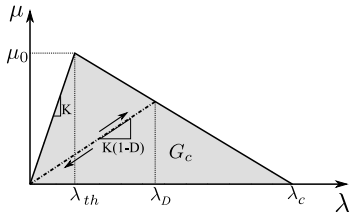

b)

Fig. 3. Bilinear cohesive law used in the analyses, [77].

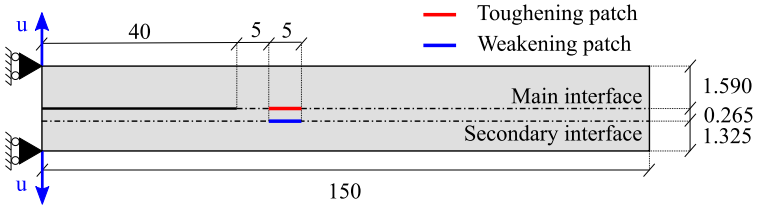

Fig. 4. Specimen, with an interface weakening or toughening patch, and boundary conditions used in the analyses. Units in [mm].

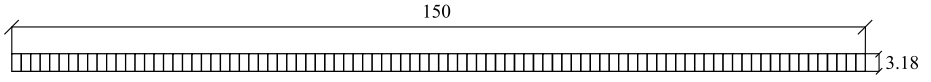

Fig. 5. Mesh of A-FNM elements used for the analyses. Units in [mm].

Table 1
Base material properties used in the analyses [81–83].

Material properties			Interface properties		
E_{11}	120	[GPa]	G_{Ic}	260	[N/m]
$E_{22} = E_{33}$	10.5	[GPa]	G_{IIc}	1002	[N/m]
$G_{12} = G_{13}$	5.3	[GPa]	τ_{I0}	30	[MPa]
G_{23}	3.5	[GPa]	τ_{II0}	60	[MPa]
$\nu_{12} = \nu_{13}$	0.3	[–]	η	2.73	[–]
ν_{23}	0.51	[–]	K	30e6	[N/mm^3]

baseline fracture properties to limit the number of simulations. The following nomenclature is used in the analyses:

$(G_c \cdot n, \tau_0 \cdot m) \Longrightarrow$ Interface toughening patch with G_c and τ_0 multiplied by a factor of n and m, respectively

$(G_c/n, \tau_0/m) \Longrightarrow$ Interface weakening patch with G_c and τ_0 divided by n and m, respectively

Remark, that G_{Ic} and G_{IIc} are scaled equally with the factor n, and τ_{I0} and τ_{II0} are scaled equally with the factor m. In the B–K criterion G_c and τ_0 at mixed mode conditions also scale linearly with the same factor as the pure mode quantities G_{cI}, G_{cII}, τ_{0I}, and τ_{0II}. A set of 50 different configurations featuring an interface toughening or weakening patch are analysed by varying the integer multipliers m and n independently from 1 to 5. Only the patched interface G_c and τ_0 parameters are modified, while keeping the other interface properties at the baseline values $(G_c \cdot 1, \tau_0 \cdot 1)$.

All the numerical tests performed use the material properties defined in Table 1. Note, that the cohesive properties in Table 1 are used at every cohesive interface of the model outside of the interface weakening or toughening patches. In the patched areas, the properties are modified according to the specification of each analysis. The mesh of A-FNM elements is shown in Fig. 5. The relation between cohesive properties proposed in [80] is used to obtain energetically consistent results under mixed-mode conditions. The ARS parameters are set up such that there is always a single refined extra element at each crack tip in the damage growth direction. A cohesive SE size of 0.083 mm in the longitudinal direction is specified meaning that a minimum of 4 cohesive SEs are discretizing each Damage Process Zone (DPZ) during the analysis. The fine mesh is required to obtain smooth results as some of the analyses feature a small DPZ due to the high onset traction in the patch area. The reader is referred to [79] for further details on the selection of the adaptive refinement method parameters.

Table 2
Outcome results matrix for the interface toughening patch cases. Note, that rows correspond to analyses with the same G_c and columns with the same τ_0.

	$\tau_0 \cdot 1$	$\tau_0 \cdot 2$	$\tau_0 \cdot 3$	$\tau_0 \cdot 4$	$\tau_0 \cdot 5$
$G_c \cdot 1$	Outcome 1	Outcome 1	Outcome 1	Outcome 1	Outcome 1
$G_c \cdot 2$	Outcome 1	Outcome 2	Outcome 2	Outcome 2	Outcome 2
$G_c \cdot 3$	Outcome 1	Outcome 3	Outcome 3	Outcome 3	Outcome 3
$G_c \cdot 4$	Outcome 1	Outcome 3	Outcome 3	Outcome 3	Outcome 3
$G_c \cdot 5$	Outcome 1	Outcome 3	Outcome 3	Outcome 3	Outcome 3

Table 3
Outcome results matrix for the interface weakening patch cases. Note, that rows correspond to analyses with the same G_c and columns with the same τ_0.

	$\tau_0/1$	$\tau_0/2$	$\tau_0/3$	$\tau_0/4$	$\tau_0/5$
$G_c/1$	Outcome 1	Outcome 1	Outcome 1	Outcome 1	Outcome 2
$G_c/2$	Outcome 1	Outcome 2	Outcome 2	Outcome 2	Outcome 2
$G_c/3$	Outcome 1	Outcome 2	Outcome 2	Outcome 2	Outcome 2
$G_c/4$	Outcome 1	Outcome 2	Outcome 2	Outcome 2	Outcome 2
$G_c/5$	Outcome 1	Outcome 2	Outcome 2	Outcome 2	Outcome 2

4. Results

The results from the different analyses with either an interface toughening or weakening patch are gathered in this section and organized in three parts. Firstly, an overview of the general response of the analyses is given, outlining the commonalities between them. Then, a detailed qualitative analysis of the mechanisms behind the initiation of multiple delaminations is provided for both interface weakening and toughening patch approaches. Later, the propagation stage after the initiation of multiple delaminations is analysed. Finally, parameter studies show the effect of changing the laminate material, the thickness of the lamina between the main and secondary interfaces, or the length of the patch. Remark, that animations of the deformed mesh, mode decomposed tractions and damage state variable evolution can be downloaded in the online version of the paper.

4.1. General response

Three clear stages can be defined in the load–crack mouth opening displacement (CMOD) equilibrium curves of the analyses shown in Figs. 6 and 7. The CMOD is defined as $(2 \cdot u)$, where the displacement u is shown in Fig. 4. All the analyses start with a single delamination stage ①, shown in Fig. 8(a), followed by the potential initiation of multiple delaminations in stage ②. This second stage is characterized by a variation of the structure response with toughening and force drop phases, compared to the single delamination case. The specimens with an interface toughening patch show a higher force peak while the specimens featuring an interface weakening patch contain a small force drop at the beginning of the load–displacement curve toughening part at stage ②. The behaviour at the propagation stage of the analyses ③ is determined by whether multiple delaminations have been initiated and which of the crack tips are propagating. For the interface toughening patch analyses, three outcomes are possible:

- Outcome (1) multiple delaminations are not initiated (Fig. 8(b)).
- Outcome (2) multiple delaminations are initiated and propagation occurs in a crack tip located at the secondary interface together with the initial crack tip at the main interface as displayed in Fig. 8(c).
- Outcome (3) multiple delaminations are initiated and propagation occurs in the two crack tips initiated at the secondary interface as shown in Fig. 8(d).

The same is valid for the interface weakening patch analyses with the difference that only outcome (2) is possible (Fig. 8(c)) when multiple delaminations are initiated. A compilation of the outcome from the 50 analyses organized in a matrix form in Tables 2 and 3, where the rows correspond to analyses with constant G_c while columns correspond to analyses with constant τ_0.

4.2. Initiation of multiple delaminations

The initiation of multiple delaminations plays a critical role in the toughening effect of the structure. Results of the analyses show that multiple delaminations are created by a combination of damage initiation and the promotion of damage growth, i.e. increase in the amount and extension of damage once initiation has occurred. Damage initiation is directly linked to the modification of the onset traction in the interface weakening and toughening patches. The modification of the critical energy release rate produces the growth of damage and eventual initiation of multiple delaminations. However, some differences between the multiple delaminations initiation mechanisms arise between the interface toughening and weakening patch analyses.

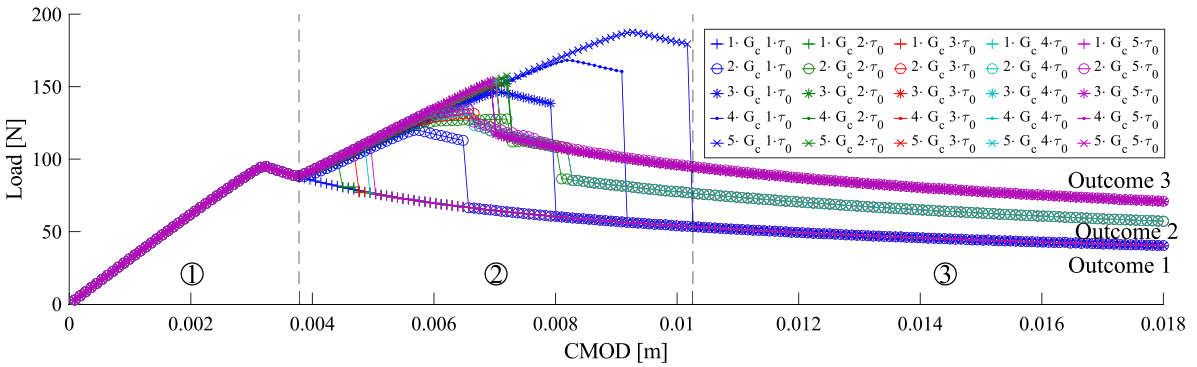

Fig. 6. Load–CMOD equilibrium curves of the analyses using an interface toughening patch.

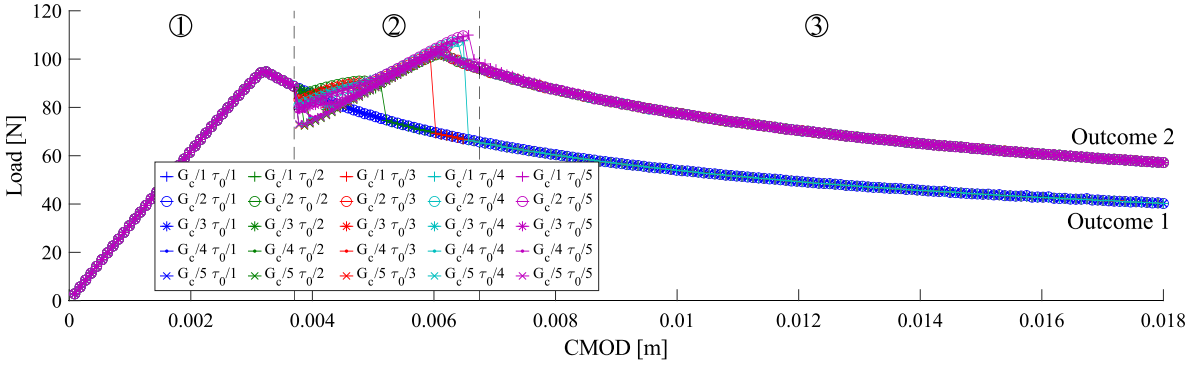

Fig. 7. Load–CMOD equilibrium curves of the analyses using an interface weakening patch.

A metric referred to as normalized traction is used to visualize the tractions during the initiation of multiple delaminations. The normalized traction $\tilde{\mu}$ is defined as:

$$\tilde{\mu} = \frac{\mu}{\mu_0} \tag{1}$$

$$\mu_0 = \sqrt{(\tau_{I0})^2 + [(\tau_{II0})^2 - (\tau_{I0})^2]B^{\eta}} \tag{2}$$

where μ is the one-dimensional equivalent cohesive traction as defined in Fig. 3, and the cohesive onset traction μ_0 is defined following a form of the Benzeggagh–Kenane (B–K) criterion, taking into account the mode mixity parameter B [77]. The normalized traction includes the effect that the local mode mixity has on the cohesive traction and the onset traction value τ_0, in a single metric. Remark, that damage initiation occurs when the normalized traction reaches a value of $\tilde{\mu} = 1$. In addition, the energetic equivalent damage variable D_e as presented in [83–86] is used to visualize the damage based on the relative energy dissipation in the CZ because it behaves linearly in terms of the separation norm λ_D:

$$D_e = \frac{G_c - w_r}{G_c} = 1 - \frac{\lambda_c(1-D)K\lambda_D}{2G_c} \tag{3}$$

where w_r is the specific remaining ability to do non-conservative work, and λ_D, λ_c are defined in Fig. 3.

4.2.1. Interface toughening patch

As seen in Fig. 6 and Table 2, solely increasing the interface toughness (G_c) or onset traction (τ_0) does not result in initiation of multiple delaminations. A load–displacement curve is shown in Fig. 9(a) for the case of a toughening patch with increased onset traction ($G_c \cdot 1, \tau_0 \cdot 3$). Two points of interest are highlighted in Fig. 9(a): Just before the initial crack enters the toughening patch ①, and when the main crack tip is about to overcome the patched area without initiating multiple delaminations ②. Figs. 9(b) and 9(c) show the distribution of the normalized traction and damage variable D_e at the two points of interest shown in Fig. 9(a) for the analysis ($G_c \cdot 1, \tau_0 \cdot 3$), in which only the onset tractions are increased. Notice, that the traction profile at ① shown in Fig. 9 contains one crack tip located at approximately 0.045 m, where the damage D_e goes to 0. At point ①, the normalized traction profile at the main interface is reproduced on the secondary interface as seen in Fig. 9(b) with a reduction in the peak value due to the elastic substrate separating both interfaces. At the point of interest ②, i.e. when the main crack front enters the interface toughening patch, the normalized traction at the main interface increases with the subsequent increase in the traction profile reproduced at the

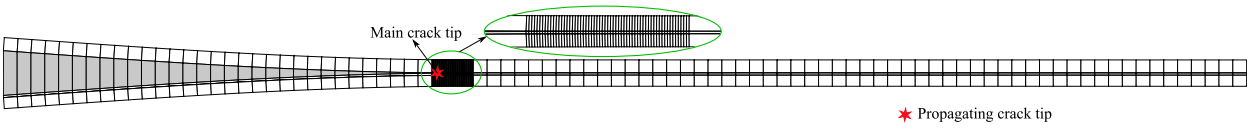

(a) Single delamination propagation stage.

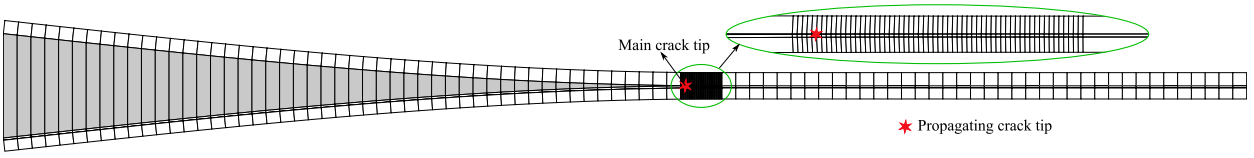

(b) Outcome 1: No initiation of multiple delaminations

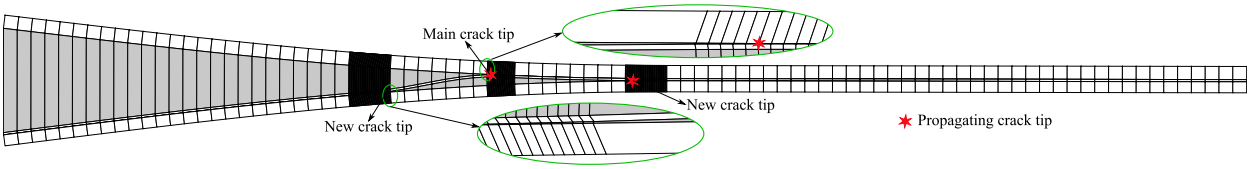

(c) Outcome 2: Propagation of the main interface crack tip and the rightmost secondary interface crack tip.

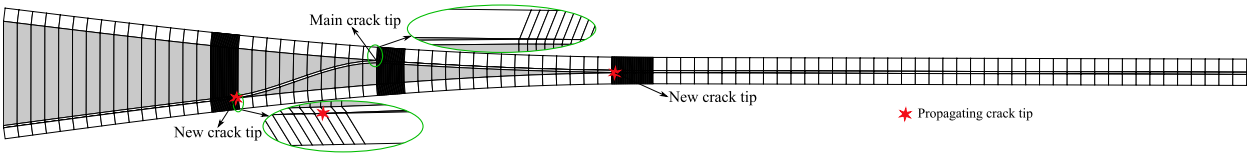

(d) Outcome 3: Propagation of the newly initiated crack tips at the secondary interface.

Fig. 8. Deformed mesh at (a) single delamination stage, (b) end of the analyses with outcome 1, (c) end of the analyses with outcome 3, and (d) end of the analyses with outcome 3. Zoomed segments with scaled deformations.

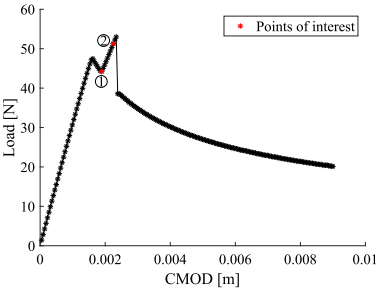

(a) Load-displacement equilibrium curve with the points of interest.

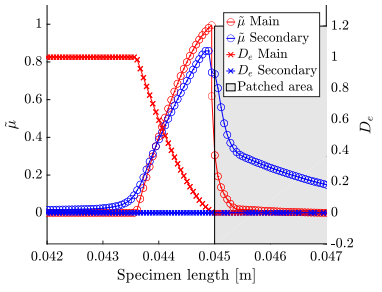

(b) Normalized traction and damage at the first point of interest.

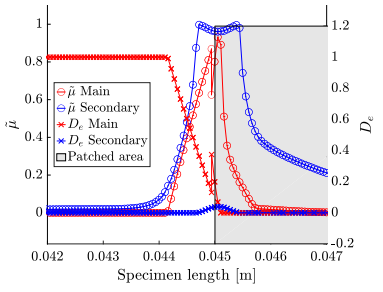

(c) Normalized traction and damage at the second point of interest.

Fig. 9. Results from the analysis ($Gc \cdot 1$, $\tau_0 \cdot 3$).

secondary interface. As the secondary interface conserves the nominal onset traction listed in Table 1, damage is initiated as shown in Fig. 9(c) where normalized traction values are close to 1. However, the quantity of damage and the extension of the damaged region is too small to initiate multiple delaminations. Remark, that the discontinuity in the damage and traction profiles is produced by the change in the interface properties between the standard and patched interface.

The results from the analysis ($G_c \cdot 3, \tau_0 \cdot 3$) in Fig. 6 and Table 2 show that multiple delaminations are initiated in the secondary interface. Fig. 10 displays the normalized tractions and damage variable D_e for the two points of interest shown in Fig. 10(a). As expected, just before the main crack front enters the interface toughening patch (point ① in Fig. 10(a)) the traction profile (Fig. 10(b)) is the same as for the analysis ($G_c \cdot 1, \tau_0 \cdot 3$). However, at point ② of Fig. 10(a) the traction profile shows a widened damaged area in which the damage value has also been increased (Fig. 10(c)). This is a result of the secondary interface trying to replicate the traction profile in the main interface, which now features an increased interface toughness, resulting in a longer DPZ and therefore a larger damaged onset area on the secondary interface. The increased DPZ creates a camel-like shape in the

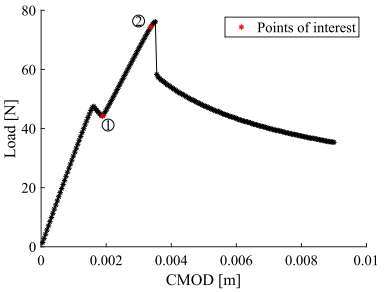

(a) Load-displacement equilibrium curve with the points of interest.

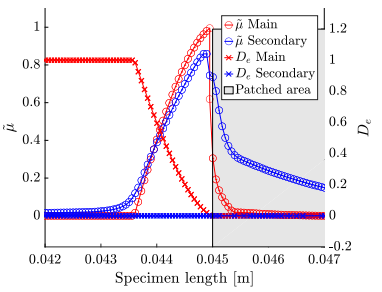

(b) Normalized traction and damage at the first point of interest.

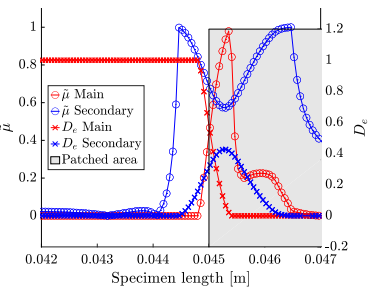

(c) Normalized traction and damage at the second point of interest.

Fig. 10. Results from the analysis ($Gc \cdot 3$, $\tau_0 \cdot 3$).

normalized traction profile of the secondary interface, which is caused by the high damage state (Fig. 10(c)). Eventually, the full damage state is reached, thus creating two separated crack fronts in the secondary interface.

The same mechanism is observed for all the analyses with an interface toughening patch that results in multiple delaminations being onset. Firstly, the increase in the traction value in the main interface is reproduced in the secondary interface. As the secondary interface properties are unmodified, the lower onset traction values (τ_{I0} and τ_{II0}) than the ones at the main interface produce damage initiation. If a sufficiently large toughness (critical energy release rate G_c) in the main interface toughening patch is achieved, the damaged area will be large enough to enable the initiation of two independent crack fronts, hence multiple delaminations.

4.2.2. Interface weakening patch

A similar mechanism of damage initiation occurs in the interface weakening patch cases. Equivalently to the interface toughening patch case, Table 3 shows that only reducing the toughness by modifying G_c does not produce multiple delaminations. However, a substantial reduction of the onset traction τ_0 results in the initiation of multiple delaminations as can be seen in the analysis ($G_c/1, \tau_0/5$). Fig. 11 shows the results of the analysis ($G_c/1, \tau_0/2$) in which an interface weakening patch is used that halves the onset traction τ_0 of the interface in the patched area. Figs. 11(b)–11(d) show the traction norm $\tilde{\mu}$ and damage variable D_e for the three points of interest marked in Fig. 11(a). Just before the main crack front reaches the interface weakening patch at point ①, the traction profile from the main interface is reproduced at the secondary interface, as in the interface toughening patch case (Fig. 11(b)). However, in the interface weakening patch case, the normalized traction profile in the main interface is mostly unaltered when the patched region is reached at point ② as can be seen in Fig. 11(c). As the onset traction τ_0 in the secondary interface is reduced in the interface weakening patch area, damage is initiated as can be observed by the large partially damaged region in the secondary interface in Fig. 11(c). However, this partially damaged region is not enough to initiate multiple delaminations because the unmodified G_c requires the dissipation of more energy before the complete formation of two new crack tips. As a result, the main crack tip overcomes the interface weakening patch area without the initiation of multiple delaminations at point ③ as can be seen in Fig. 11(d).

Simultaneously reducing τ_0 and G_c successfully triggers multiple delaminations as seen in Fig. 7 and Table 3. At the first point of interest shown in Fig. 12(a) the same situation as for the analysis ($G_c/1, \tau_0/2$) is observed (Fig. 12(b)). However, as the toughness is reduced, the level of damage in the secondary interface increases forming a similar camel-back shape in the normalized traction profile (Fig. 12(b)) as the one observed in the interface toughening patch case on Fig. 10(c), which eventually results in the initiation of multiple delaminations with two fully formed crack fronts and a fully damaged region in between them (see Fig. 12(d) ③ at point ③). However, unlike the interface toughening patch case, the newly formed crack fronts and the previously existing one need to enlarge their DPZ to transition from the weakened patch to the original interface properties (Fig. 12(e) ⑦), which creates a toughening effect in the load–displacement curve shown in Fig. 12(a) between ③ and ④.

The same mechanisms are observed in the other analyses featuring an interface weakening patch that result in the initiation of multiple delaminations. The decrease in τ_0 onsets damage, followed by the propagation and increase of the damage driven by the lowered G_c. Such reduction means that less energy is necessary to propagate damage in the interface weakening patch, which allows the initiation of multiple delaminations.

4.3. Propagation

After the multiple delaminations initiation stage, the propagation stage ③ takes place as seen in Figs. 6 and 7. The objective of initiating multiple delaminations is to achieve a propagation stage with higher energy dissipation as this translates into better load carrying capabilities and slower crack growth in the analysis pseudo-time. To evaluate the energy dissipation capabilities of the structure, the energy dissipation rate $\dot{\omega}_{diss}$ is defined as:

$$\dot{\omega}_{diss} = \frac{d\omega}{dCMOD} \approx \frac{\Delta\omega}{\Delta CMOD} \tag{4}$$

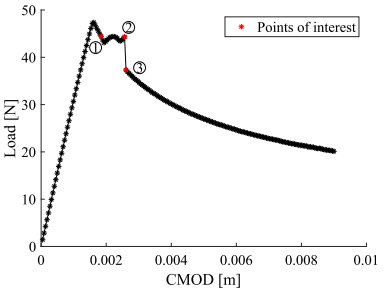

(a) Load-displacement equilibrium curve with the points of interest.

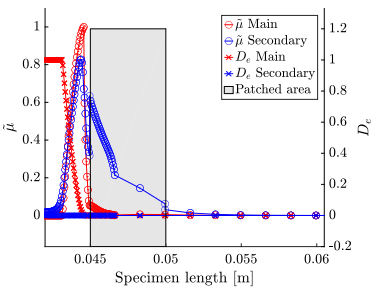

(b) Normalized traction and damage at the first point of interest.

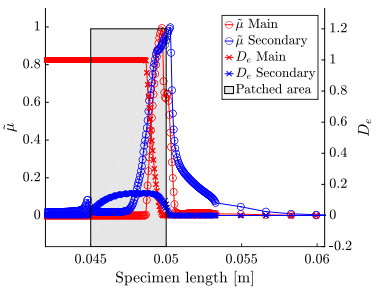

(c) Normalized traction and damage at the second point of interest.

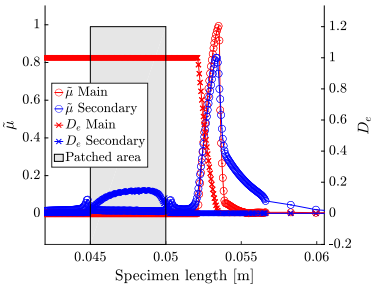

(d) Normalized traction and damage at the third point of interest.

Fig. 11. Results from the analysis ($Gc/1$, $\tau_0/2$).

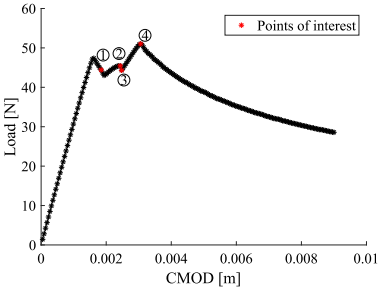

(a) Load-displacement equilibrium curve with the points of interest.

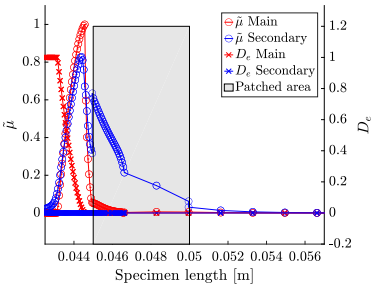

(b) Normalized traction and damage at the first point of interest.

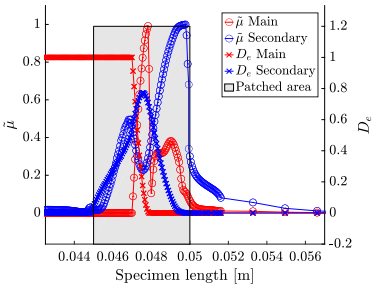

(c) Normalized traction and damage at the second point of interest.

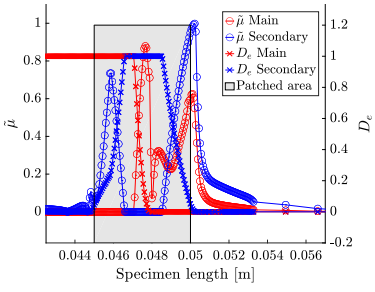

(d) Normalized traction and damage at the third point of interest.

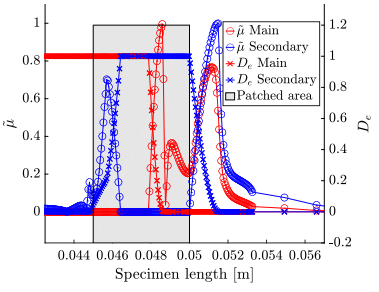

(e) Normalized traction and damage at the fourth point of interest.

Fig. 12. Results from the analysis ($Gc/2$, $\tau_0/2$).

where $\Delta\omega$ is the energy dissipated in an increment of Crack Mouth Opening Displacement $\Delta CMOD$, where CMOD is defined in Section 4.1. Although the fine cohesive discretization provided by the adaptive refinement results in smooth equilibrium curves as

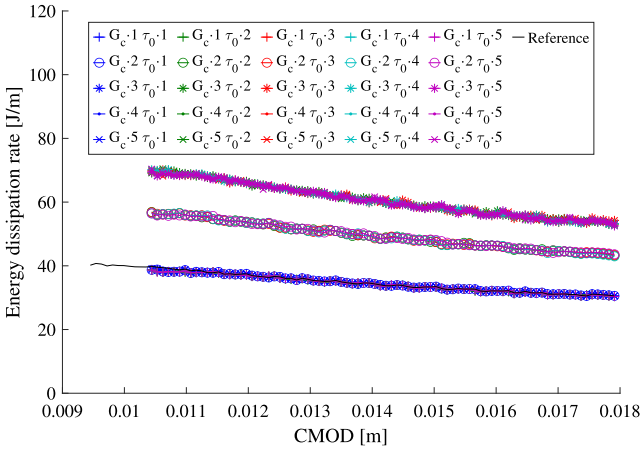

Fig. 13. Energy dissipation rate with respect to crack mouth opening for the interface toughening patch analyses in the propagation stage (3).

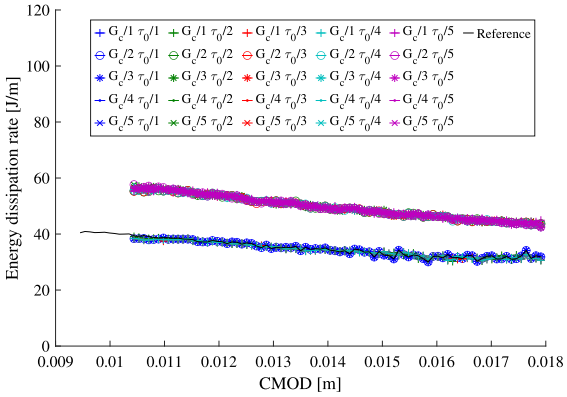

Fig. 14. Energy dissipation rate with respect to crack mouth opening for the interface weakening patch analyses in the propagation stage (3).

seen in Figs. 6 and 7, small oscillations inherent to the cohesive formulations during the propagation of the delamination cracks are still present. As such oscillations are amplified by the differentiation of the equilibrium curve, a moving average filter is used with a window of 10 data points in the propagation stage of the equilibrium curve. Remark, that an alternative approach can be used for the calculation of the dissipated energy by using the energy release rate calculated with the individual crack tip J-Integral as done in [86,87] and the crack growth information.

4.3.1. Interface toughening patch

Fig. 13 shows the energy dissipation rate for the analyses with an interface toughening patch after the eventual initiation of multiple delaminations. A downwards trend of the energy dissipation is observed as the force is being reduced under displacement control conditions. Three levels of energy dissipation rates are observed corresponding to the three possible outcomes of the analyses: (1) No initiation of multiple delaminations (Fig. 8(b)), (2) Propagation of the main interface crack tip and the leftmost secondary interface crack tip (Fig. 8(c)) and (3) Propagation of crack tips at the secondary interface (Fig. 8(d)). If a large interface toughness for the interface toughening patch is used, the main delamination is arrested leading to scenario (3) whereas if the increase in toughness is sufficient to create multiple delaminations but does not arrest the main crack, scenario (2) will occur.

4.3.2. Interface weakening patch

Fig. 14 shows the energy dissipation rate for the analyses with the interface weakening patch on the secondary interface. The propagation stage differs from the interface toughening patch cases as only outcome (2) is possible, resulting in a continued propagation of the main crack tip together with the propagation of the rightmost newly formed crack tip on the secondary interface. The reason is that outcome (3) shown in Fig. 8(d) is only possible with a toughening of the main interface which arrests the main crack. Since the main interface is unaltered in the interface weakening patch analyses, outcome (3) is not possible.

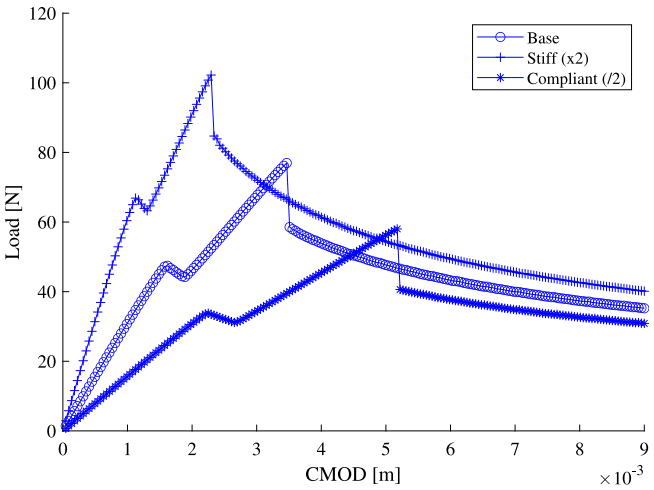

Fig. 15. Load–displacement curve for different laminate stiffness.

4.4. Influence of laminate material, thickness, and patch length

In Sections 4.1 to 4.3 the effect of varying the strength and toughness of the patches while keeping all other material and structural parameters fixed were presented. In this section, additional investigations are presented to show the effect of changing the laminate material, the thickness of the intermediate lamina between the main and secondary interfaces, and the length of the interface toughening/weakening patches. In these studies the same interface toughening patch configuration ($G_c \cdot 3, \tau_0 \cdot 3$) is used to restrict the number of analyses, however, the same general behaviour has been observed for the other patch material properties.

4.4.1. Laminate material properties

Fig. 15 shows the results of 3 tests in which the laminate stiffness is varied while having an interface toughening patch ($G_c \cdot 3, \tau_0 \cdot 3$) configuration. The material listed in Table 1 is used as the baseline, while a stiff (twice the baseline stiffness) and compliant (half the baseline elastic stiffness) laminate material is defined for the remaining. The results presented in Fig. 15, show a low energy dissipation for compliant specimens, a behaviour also observed for a single delamination case. The multiple delaminations initiation capabilities are not affected in any manner by changing the stiffness of the laminate.

4.4.2. Thickness of the intermediate lamina

The thickness of the intermediate lamina between the main and secondary interfaces affects the onset and the propagation phases of the analyses. A set of 10 analyses with an intermediate lamina ranging from 0.2 mm to 2 mm have been simulated using the specimen shown in Fig. 4. Remark, the overall thickness of the laminate is kept constant. The material listed in Table 1 with an interface toughening patch configuration of ($G_c \cdot 3, \tau_0 \cdot 3$) is applied. As stated in Section 4.2, damage initiation is a consequence of the reproduction of the tractions at the secondary interface originated by the crack tip propagating in the main interface. As observed in Fig. 16(a), increasing the thickness of the intermediate lamina reduces the peak value of the tractions produced at the secondary interface. Therefore, a larger thickness reduces the ability to onset damage at the secondary interface and thus initiate multiple delaminations. Fig. 16(b), shows that the intermediate lamina thickness also affects the propagation phase. A larger thickness causes an increase in the dissipated energy during the propagation phase.

4.4.3. Patch length

The effect of different lengths of the interface toughening/weakening patches has also been studied. The tests use the same specimen and material properties as shown in Fig. 4 and Table 1, respectively. The results show that, as expected, a shortening of the patch decreases the likelihood of multiple delaminations. This effect is difficult to quantify and visualize, but a critical length for each laminate material and intermediate layer thickness configuration exists. For patch lengths lower than this critical value, damage is initiated but multiple delaminations are not fully developed.

5. Discussion

Introducing an interface toughening patch in the main interface or a weakening one in the secondary interface can initiate multiple delaminations resulting in a toughening of the structure response. Nevertheless, there are some advantages and disadvantages in both approaches that are worth discussing. Firstly, the structure experiences an increased ability to sustain higher force and prescribed displacements in both weakening and toughening cases. For a force loading case, there is an engineering interest

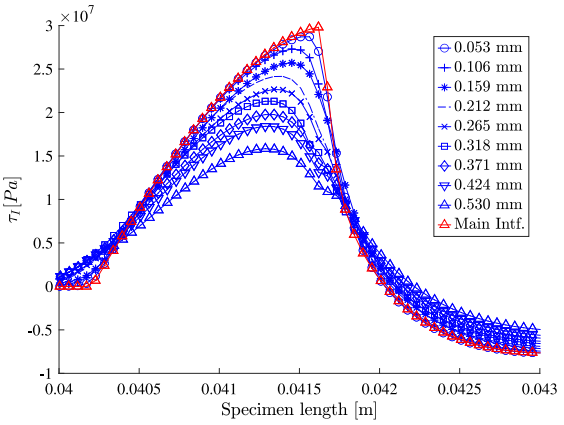

(a) Traction profile at the secondary interface for different main-secondary interfaces spacing at the initial single delamination propagation phase.

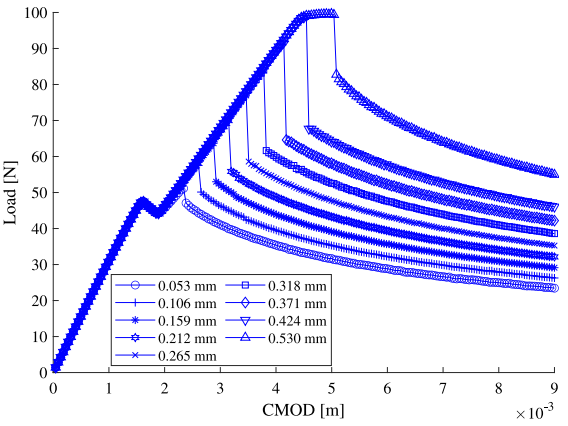

(b) Load-displacement curve for different spacing between the main and secondary interfaces.

Fig. 16. Results from analyses featuring different spacing between the main and the secondary interfaces, using an interface toughening patch ($G_c \cdot 3, \tau_0 \cdot 3$).

in increasing the maximum load that the structure can sustain before crack propagation occurs, potentially triggering an unstable crack growth scenario. The structure featuring a toughening patch is capable of carrying forces 95% higher than the original peak force when multiple delaminations are initiated (see Fig. 6). For the interface weakening patch cases, a force peak value increase of around 15% of the original maximum force can be achieved (Fig. 7). Under a situation of prescribed displacement loading, the main engineering interest is improving the load-carrying capacities of the structure. For the propagation phase, the structures with a toughening patch obtain an increase of their load-carrying capacity around 100% for the outcome 3 cases, and around 65% for the outcome 2 cases (Fig. 6). As the weakening patch can only result in outcome 1 or 2, a potential increase in the load-carrying capabilities during the propagation phase around 65% is observed (Fig. 7). Therefore, both interface weakening and toughening patches increase the overall dissipated energy while also increasing the peak load, and the load-carrying capabilities during the delamination propagation phase. Both approaches are useful for application in damage-tolerant designs. However, the interface toughening patch offers a larger improvement of the peak load and load carrying capabilities of the structure. It is important to note, that the interface toughening patch approach needs a higher degree of precision when choosing the strength and toughness parameters to achieve the desired result among the two possible multiple delaminations outcomes displayed in Figs. 8(c) and 8(d). With the weakening approach, the initiation of multiple delaminations is sufficient to obtain a predictable response during the propagation phase.

Regarding the applicability of this approach for a variety of laminate materials, laminate thicknesses, and patch lengths, the studies presented in Section 4.4 show different degrees of influence of such parameters. Changing the laminate stiffness has the same effect as for a single delamination case: A more compliant material reduces the energy dissipation lowering the crack extension for a given increment in pseudo solution time. However, even for a compliant material an increase in the dissipation energy is still achieved thus toughening the structure against delamination. The distance between the main and secondary interfaces affects the initiation of multiple delaminations and the amount of energy that is dissipated as shown in Fig. 16(b). During the multiple delaminations initiation phase, Fig. 16(a) shows that the traction peak of the reproduced traction profile from the main interface to the secondary interface is smaller. This means that there are two critical onset traction values for the weakening and toughening patch materials linked to damage initiation at the secondary interface. In the case of the toughening patch, if the onset traction is higher than such critical value, damage will be initiated at the secondary interface. For the weakening patch case, if the onset traction of the patch material is lower than the critical value, damage at the secondary interface will also be initiated. The critical values depend on the laminate material properties and the distance separating the interfaces. This is also observed in the equilibrium curves shown in Fig. 16(b) where a higher force and displacement level is needed to initiate the multiple delaminations for large interfaces distances. Remark, that a too large distancing between the interfaces results in damage initiation at the secondary interface without initiation of multiple delaminations. The propagation phase is also affected as can be observed in the final stages of the analyses shown on Fig. 16(b). The modified thicknesses of the sublaminate bridging the two interfaces originated after multiple delaminations initiation provoke different local energy dissipation at every crack tip. Such effect is difficult to predict exactly at the local crack tip level because of the high degree of interaction between the different delamination fronts. However, it can clearly be observed that smaller spacing between the main and secondary interface results in lower energy dissipation.

6. Conclusion

A numerical study on the feasibility of toughened laminated composite structures against delamination propagation using interface weakening or toughening material patches that initiate multiple delaminations is presented. The analyses are performed

using the adaptive floating node-based finite element formulation from [79]. Firstly, a set of 50 parameter studies are presented studying patches featuring different combinations of strength and toughness. The analyses show that both weakening and toughening interface patches can initiate multiple delaminations. Results also demonstrate that a toughening on the response is observed, with the interface toughening patch approach dissipating more energy than the interface weakening patches. Secondly, the effect of changing the laminate stiffness, the spacing between the main and secondary interfaces, and the patch length is studied. The three variables are observed to affect the results with the spacing between the interfaces being the most prominent one.

A discussion on the applicability of the presented toughening strategy against delamination is presented focusing on the capability of the patched structure to improve the response to displacement or force loading. Both interface weakening and toughening patches improve the capability of the structure to undergo higher loads than the baseline. However, the interface toughening patch approach has a higher increase in the peak force and displacement when multiple delaminations are initiated. The main advantage of using interface weakening patches is that the response of the structure can be controlled more easily, obtaining the same outcome for a wide range of patch strength and critical energy release rates.

Further experimental work is needed to validate the numerical results presented in this work. For this purpose, the authors consider several options for the creation of the toughening patch. These include placing a small toughening interleave, stitching two layers on the toughening patch section, or dispersing carbon nanotubes on the same region. As for the weakening patch, a short layer of material with reduced adhesive capabilities or the contamination of the weakening patch area would effectively reduce the interface mechanical properties as desired.

Promising results are obtained in the performed analyses, making the presented approach an interesting option to achieve damage tolerance by toughening laminated composite structures against delamination propagation.

CRediT authorship contribution statement

Guillem Gall Trabal: Writing – review & editing, Writing – original draft, Visualization, Validation, Project administration, Methodology, Investigation, Formal analysis, Conceptualization. **Brian Lau Verndal Bak:** Writing – review & editing, Supervision, Investigation, Funding acquisition, Conceptualization. **Boyang Chen:** Writing – review & editing, Validation, Conceptualization. **Simon Mosbjerg Jensen:** Writing – review & editing, Validation, Conceptualization. **Esben Lindgaard:** Writing – review & editing, Validation, Supervision, Funding acquisition, Conceptualization.

Declaration of competing interest

The authors declare that they have no known competing financial interests or personal relationships that could have appeared to influence the work reported in this paper.

Data availability

Data will be made available on request.

Acknowledgements

This work is supported by the Talent Management Programme at Aalborg University, Denmark (Internal grant number: 771120). This support is gratefully acknowledged.

Appendix A. Supplementary data

Supplementary material related to this article can be found online at https://doi.org/10.1016/j.engfracmech.2022.108730.

References

[1] Pagano N, Schoeppner G. Delamination of polymer matrix composites: Problems and assessment. In: Kelly A, Zweben C, editors. Comprehensive composite materials. Oxford: Pergamon; 2000, p. 433–528. http://dx.doi.org/10.1016/B0-08-042993-9/00073-5.

[2] Hallett SR, Jiang WG, Khan B, Wisnom MR. Modelling the interaction between matrix cracks and delamination damage in scaled quasi-isotropic specimens. Compos Sci Technol 2008;68(1):80–9. http://dx.doi.org/10.1016/j.compscitech.2007.05.038.

[3] Zubillaga L, Turon A, Renart J, Costa J, Linde P. An experimental study on matrix crack induced delamination in composite laminates. Compos Struct 2015;127:10–7. http://dx.doi.org/10.1016/j.compstruct.2015.02.077.

[4] Ogin S, Brøndsted P, Zangenberg J. 1 - Composite materials: constituents, architecture, and generic damage. In: Talreja R, Varna J, editors. Modeling damage, fatigue and failure of composite materials. Woodhead publishing series in composites science and engineering, Woodhead Publishing; 2016, p. 3–23. http://dx.doi.org/10.1016/B978-1-78242-286-0.00001-7.

[5] Cantwell WJ, Morton J. The significance of damage and defects and their detection in composite materials: A review. J Strain Anal Eng Des 1992;27(1):29–42. http://dx.doi.org/10.1243/03093247V271029.

[6] Lindgaard E, Bak BLV. Experimental characterization of delamination in off-axis GFRP laminates during mode I loading. Compos Struct 2019;220(February):953–60. http://dx.doi.org/10.1016/j.compstruct.2019.04.022.

[7] Jensen SM, Martos MJ, Bak BL, Lindgaard E. Formulation of a mixed-mode multilinear cohesive zone law in an interface finite element for modelling delamination with R-curve effects. Compos Struct 2019;216(February):477–86. http://dx.doi.org/10.1016/j.compstruct.2019.02.029.

[8] Jensen S, Martos M, Lindgaard E, Bak B. Inverse parameter identification of n-segmented multilinear cohesive laws using parametric finite element modeling. Compos Struct 2019;225:111074. http://dx.doi.org/10.1016/j.compstruct.2019.111074.

[9] Giurgiutiu V. Structural health monitoring of aerospace composites. Elsevier Academic Press; 2015.

[10] Solaimurugan S, Velmurugan R. Influence of in-plane fibre orientation on mode I interlaminar fracture toughness of stitched glass/polyester composites. Compos Sci Technol 2008;68(7):1742–52. http://dx.doi.org/10.1016/j.compscitech.2008.02.008.

[11] Sebaey T, González E, Lopes C, Blanco N, Maimí P, Costa J. Damage resistance and damage tolerance of dispersed CFRP laminates: Effect of the mismatch angle between plies. Compos Struct 2013;101:255–64. http://dx.doi.org/10.1016/j.compstruct.2013.01.026.

[12] Hwang W, Han K. Interlaminar fracture behavior and fiber bridging of glass-epoxy composite under mode I static and cyclic loadings. J Compos Mater 1989;23(4):396–430.

[13] Spearing S, Evans A. The role of fiber bridging in the delamination resistance of fiber-reinforced composites. Acta Metall Mater 1992;40(9):2191–9. http://dx.doi.org/10.1016/0956-7151(92)90137-4.

[14] Gong Y, Tian D, Cao T, Zhao L, Zhang J, Hu N, Zhang C. An R-curve effect-included delamination growth criterion for mixed-mode I/II delamination predictions of composite laminates. Compos Struct 2022;295:115846. http://dx.doi.org/10.1016/j.compstruct.2022.115846.

[15] Liu C, Gong Y, Gong Y, Li W, Liu Z, Hu N. Mode II fatigue delamination behaviour of composite multidirectional laminates and the stress ratio effect. Eng Fract Mech 2022;264:108321. http://dx.doi.org/10.1016/j.engfracmech.2022.108321.

[16] Kim J, Baillie C, Poh J, Mai Y-W. Fracture toughness of CFRP with modified epoxy resin matrices. Compos Sci Technol 1992;43(3):283–97. http://dx.doi.org/10.1016/0266-3538(92)90099-O.

[17] Yan C, Xiao K, Ye L, Mai Y-W. Numerical and experimental studies on the fracture behavior of rubber-toughened epoxy in bulk specimen and laminated composites. J Mater Sci 2002;37(5):921–7.

[18] Ratna D. Modification of epoxy resins for improvement of adhesion: a critical review. J Adhes Sci Technol 2003;17(12):1655–68. http://dx.doi.org/10.1163/156856103322396721.

[19] DeCarli M, Kozielski K, Tian W, Varley R. Toughening of a carbon fibre reinforced epoxy anhydride composite using an epoxy terminated hyperbranched modifier. Compos Sci Technol 2005;65(14):2156–66. http://dx.doi.org/10.1016/j.compscitech.2005.05.003.

[20] Verrey J, Winkler Y, Michaud V, Månson J-A. Interlaminar fracture toughness improvement in composites with hyperbranched polymer modified resin. Compos Sci Technol 2005;65(10):1527–36. http://dx.doi.org/10.1016/j.compscitech.2005.01.005.

[21] Bagheri R, Marouf B, Pearson R. Rubber-toughened epoxies: a critical review. J Macromol Sci C 2009;49(3):201–25.

[22] Imagawa S, Nishida H, Okubo K, Fujii T. Improvement of mode-II interlaminar fracture toughness of carbon textile composites with modified matrix of thermoplastic and thermoset epoxy-addition of glass fibers. In: IOP conference series: Materials science and engineering, Vol. 406. IOP Publishing; 2018, 012045.

[23] Drzal L, Madhukar M. Fibre-matrix adhesion and its relationship to composite mechanical properties. J Mater Sci 1993;28(3):569–610.

[24] Dilsiz N, Wightman J. Effect of acid–base properties of unsized and sized carbon fibers on fiber/epoxy matrix adhesion. Colloids Surf A 2000;164(2):325–36. http://dx.doi.org/10.1016/S0927-7757(99)00400-8.

[25] Feih S, Wei J, Kingshott P, Sørensen B. The influence of fibre sizing on the strength and fracture toughness of glass fibre composites. Composites A 2005;36(2):245–55. http://dx.doi.org/10.1016/j.compositesa.2004.06.019.

[26] Jones F. A review of interphase formation and design in fibre-reinforced composites. J Adhes Sci Technol 2010;24(1):171–202.

[27] Rich M, Drown E, Askeland P, Drzal L. Surface treatment of carbon fibers by ultraviolet light+ ozone: its effect on fiber surface area and topography. In: The 19th international conference on composite materials. 2013, p. 1196–204.

[28] Liu W, Zhang S, Li B, Yang F, Jiao W, Hao L, Wang R. Improvement in interfacial shear strength and fracture toughness for carbon fiber reinforced epoxy composite by fiber sizing. Polym Compos 2014;35(3):482–8.

[29] Downey MA, Drzal LT. Toughening of carbon fiber-reinforced epoxy polymer composites utilizing fiber surface treatment and sizing. Composites A 2016;90:687–98. http://dx.doi.org/10.1016/j.compositesa.2016.09.005.

[30] Wu Z, Yi X-S, Wilkinson A. Interlaminar fracture toughness of carbon fibre/RTM6-2 composites toughened with thermoplastic-coated fabric reinforcement. Composites B 2017;130:192–9. http://dx.doi.org/10.1016/j.compositesb.2017.08.003.

[31] Grytten F, Sørensen BF, Goutianos S, Joki RK, Jørgensen JK. A micromechanical model of fiber bridging including effects of large deflections of the bridging fibers. Compos Struct 2021;258:113405. http://dx.doi.org/10.1016/j.compstruct.2020.113405.

[32] Bullegas G, Pinho ST, Pimenta S. Engineering the translaminar fracture behaviour of thin-ply composites. Compos Sci Technol 2016;131:110–22. http://dx.doi.org/10.1016/j.compscitech.2016.06.002.

[33] Bullegas G, Benoliel J, Fenelli PL, Pinho ST, Pimenta S. Towards quasi isotropic laminates with engineered fracture behaviour for industrial applications. Compos Sci Technol 2018;165:290–306. http://dx.doi.org/10.1016/j.compscitech.2018.07.004.

[34] McCrary-Dennis MC, Okoli OI. A review of multiscale composite manufacturing and challenges. J Reinf Plast Compos 2012;31(24):1687–711.

[35] Lau K-T, Shi S-Q, Zhou L-M, Cheng H-M. Micro-hardness and flexural properties of randomly-oriented carbon nanotube composites. J Compos Mater 2003;37(4):365–76.

[36] Gojny F, Wichmann M, Köpke U, Fiedler B, Schulte K. Carbon nanotube-reinforced epoxy-composites: enhanced stiffness and fracture toughness at low nanotube content. Compos Sci Technol 2004;64(15):2363–71. http://dx.doi.org/10.1016/j.compscitech.2004.04.002, Developments in carbon nanotube and nanofibre reinforced polymers.

[37] Gao X, Liu L, Guo Q, Shi J, Zhai G. Fabrication and mechanical/conductive properties of multi-walled carbon nanotube (MWNT) reinforced carbon matrix composites. Mater Lett 2005;59(24):3062–5. http://dx.doi.org/10.1016/j.matlet.2005.05.021.

[38] Kinloch A, Masania K, Taylor A, Sprenger S, Egan D. The fracture of glass-fibre-reinforced epoxy composites using nanoparticle-modified matrices. J Mater Sci 2008;43(3):1151–4.

[39] Zhou Y, Jeelani S, Lacy T. Experimental study on the mechanical behavior of carbon/epoxy composites with a carbon nanofiber-modified matrix. J Compos Mater 2014;48(29):3659–72.

[40] Rahmanian S, Suraya A, Shazed M, Zahari R, Zainudin E. Mechanical characterization of epoxy composite with multiscale reinforcements: Carbon nanotubes and short carbon fibers. Mater Des 2014;60:34–40. http://dx.doi.org/10.1016/j.matdes.2014.03.039.

[41] Prasad N, Tola C, Coulaud M, Claes M, Lomov SV, Verpoest I, Gorbatikh L. Carbon fiber composites based on multi-phase epoxy/PES matrices with carbon nanotubes: morphology and interlaminar fracture toughness characterization. Adv Energy Mater 2016;18(12):2040–6.

[42] Joshi SC, Dikshit V. Enhancing interlaminar fracture characteristics of woven CFRP prepreg composites through CNT dispersion. J Compos Mater 2012;46(6):665–75.

[43] Li P, Liu D, Zhu B, Li B, Jia X, Wang L, Li G, Yang X. Synchronous effects of multiscale reinforced and toughened CFRP composites by MWNTs-EP/PSF hybrid nanofibers with preferred orientation. Composites A 2015;68:72–80. http://dx.doi.org/10.1016/j.compositesa.2014.09.010.

[44] Yokozeki T, Iwahori Y, Ishibashi M, Yanagisawa T, Imai K, Arai M, Takahashi T, Enomoto K. Fracture toughness improvement of CFRP laminates by dispersion of cup-stacked carbon nanotubes. Compos Sci Technol 2009;69(14):2268–73. http://dx.doi.org/10.1016/j.compscitech.2008.12.017, The Sixteenth International Conference on Composite Materials with Regular Papers.

[45] Heß H, Himmel N. Structurally stitched NCF CFRP laminates. Part 1: Experimental characterization of in-plane and out-of-plane properties. Compos Sci Technol 2011;71(5):549–68. http://dx.doi.org/10.1016/j.compscitech.2010.11.012.

[46] Shiino MY, Pelosi TS, Cioffi MOH, Donadon MV. The role of stitch yarn on the delamination resistance in non-crimp fabric: chemical and physical interpretation. J Mater Eng Perform 2017;26(3):978–86.
[47] Ravandi M, Teo W, Tran L, Yong M, Tay T. The effects of through-the-thickness stitching on the mode i interlaminar fracture toughness of flax/epoxy composite laminates. Mater Des 2016;109:659–69. http://dx.doi.org/10.1016/j.matdes.2016.07.093.
[48] Göktaş D, Kennon W, Potluri P. Improvement of Mode I interlaminar fracture toughness of stitched glass/epoxy composites. Appl Compos Mater 2017;24(2):351–75. http://dx.doi.org/10.1007/s10443-016-9560-x.
[49] Ladani RB, Ravindran AR, Wu S, Pingkarawat K, Kinloch AJ, Mouritz AP, Ritchie RO, Wang CH. Multi-scale toughening of fibre composites using carbon nanofibres and z-pins. Compos Sci Technol 2016;131:98–109. http://dx.doi.org/10.1016/j.compscitech.2016.06.005.
[50] Yasaee M, Bigg L, Mohamed G, Hallett SR. Influence of Z-pin embedded length on the interlaminar traction response of multi-directional composite laminates. Mater Des 2017;115:26–36. http://dx.doi.org/10.1016/j.matdes.2016.11.025.
[51] Mouritz A. Review of z-pinned laminates and sandwich composites. Composites A 2020;139:106128. http://dx.doi.org/10.1016/j.compositesa.2020.106128.
[52] Gong Y, Chen X, Zou L, Li X, Zhao L, Zhang J, Hu N. Experimental and numerical investigations on the mode I delamination growth behavior of laminated composites with different z-pin fiber reinforcements. Compos Struct 2022;287:115370. http://dx.doi.org/10.1016/j.compstruct.2022.115370.
[53] Mouritz A, Bannister M, Falzon P, Leong K. Review of applications for advanced three-dimensional fibre textile composites. Composites A 1999;30(12):1445–61. http://dx.doi.org/10.1016/S1359-835X(99)00034-2.
[54] Mouritz A, Baini C, Herszberg I. Mode I interlaminar fracture toughness properties of advanced textile fibreglass composites. Composites A 1999;30(7):859–70. http://dx.doi.org/10.1016/S1359-835X(98)00197-3.
[55] Pankow M, Salvi A, Waas A, Yen C, Ghiorse S. Resistance to delamination of 3D woven textile composites evaluated using End Notch Flexure (ENF) tests: Experimental results. Composites A 2011;42(10):1463–76. http://dx.doi.org/10.1016/j.compositesa.2011.06.013.
[56] Pascoe J-A, Pimenta S, Pinho ST. Interlocking thin-ply reinforcement concept for improved fracture toughness and damage tolerance. Compos Sci Technol 2019;181:107681. http://dx.doi.org/10.1016/j.compscitech.2019.107681.
[57] Ishai O, Rosenthal H, Sela N, Drukker E. Effect of selective adhesive interleaving on interlaminar fracture toughness of graphite/epoxy composite laminates. Composites 1988;19(1):49–54. http://dx.doi.org/10.1016/0010-4361(88)90543-5.
[58] Masters JE. Improved impact and delamination resistance through interleafing. In: Key engineering materials, Vol. 37. Trans Tech Publ; 1989, p. 317.
[59] Tanimoto T. Suppression of interlaminar damage in carbon/epoxy laminates by use of interleaf layers. Scr Metall Mater 1994;31(8):1073–8. http://dx.doi.org/10.1016/0956-716X(94)90529-0.
[60] Singh S, Partridge I. Mixed-mode fracture in an interleaved carbon-fibre/epoxy composite. Compos Sci Technol 1995;55(4):319–27. http://dx.doi.org/10.1016/0266-3538(95)00062-3.
[61] Lu W, Liao F, Su A, Kao P, Hsu T. Effect of interleaving on the impact response of a unidirectional carbon/epoxy composite. Composites 1995;26(3):215–22. http://dx.doi.org/10.1016/0010-4361(95)91385-I.
[62] Sohn M-S, Hu X-Z. Processing of carbon-fibre/epoxy composites with cost-effective interlaminar reinforcement. Compos Sci Technol 1998;58(2):211–20. http://dx.doi.org/10.1016/S0266-3538(97)00114-0, Australasian Special Issue on Manufacturing Processes and Mechanical Properties Characterisation of Advanced Composites.
[63] Jiang W, Tjong S, Chu P, Li R, Kim JK, Mai Y. Interlaminar fracture properties of carbon fibre/epoxy matrix composites interleaved with polyethylene terephthalate (PET) films. Polym Polym Compos 2001;9(2):141–5.
[64] Arai M, Noro Y, ichi Sugimoto K, Endo M. Mode I and mode II interlaminar fracture toughness of CFRP laminates toughened by carbon nanofiber interlayer. Compos Sci Technol 2008;68(2):516–25. http://dx.doi.org/10.1016/j.compscitech.2007.06.007.
[65] Wong DW, Lin L, McGrail PT, Peijs T, Hogg PJ. Improved fracture toughness of carbon fibre/epoxy composite laminates using dissolvable thermoplastic fibres. Composites A 2010;41(6):759–67. http://dx.doi.org/10.1016/j.compositesa.2010.02.008.
[66] Shivakumar KN, Panduranga R, Sharpe M. Interleaved polymer matrix composites-a review. In: 54th AIAA/ASME/ASCE/AHS/ASC structures, structural dynamics, and materials conference. 2013, p. 1903.
[67] Chen C, Li Y, Yu T. Interlaminar toughening in flax fiber-reinforced composites interleaved with carbon nanotube buckypaper. J Reinf Plast Compos 2014;33(20):1859–68.
[68] Daelemans L, van der Heijden S, De Baere I, Rahier H, Van Paepegem W, De Clerck K. Using aligned nanofibres for identifying the toughening micromechanisms in nanofibre interleaved laminates. Compos Sci Technol 2016;124:17–26. http://dx.doi.org/10.1016/j.compscitech.2015.11.021.
[69] Lan B, Liu Y, Mo S, He M, Zhai L, Fan L. Interlaminar fracture behavior of carbon fiber/polyimide composites toughened by interleaving thermoplastic polyimide fiber veils. Materials 2021;14(10):2695.
[70] Goutianos S, Sørensen BF. Fracture resistance enhancement of layered structures by multiple cracks. Eng Fract Mech 2016;151:92–108. http://dx.doi.org/10.1016/j.engfracmech.2015.10.036.
[71] Goutianos S, Sørensen BF. Enhancement of fracture resistance by multiple cracks in layered structures under mode I and mix mode loading. In: 21st international conference on composite materials (ICCM-21). 2017.
[72] Sørensen BF, Goutianos S. Increase of fracture resistance by the interaction of two cracks cohesive law scale effects. In: Proceedings of the 6th European conference on computational mechanics. 2018.
[73] Herráez M, Pichler N, Botsis J. Improving delamination resistance through tailored defects. Compos Struct 2020;247:112422. http://dx.doi.org/10.1016/j.compstruct.2020.112422.
[74] Tao R, Alfano M, Lubineau G. Laser-based surface patterning of composite plates for improved secondary adhesive bonding. Composites A 2018;109:84–94. http://dx.doi.org/10.1016/j.compositesa.2018.02.041.
[75] Li X, Tao R, Alfano M, Lubineau G. How variability in interfacial properties results in tougher bonded composite joints by triggering bridging. Int J Solids Struct 2020;191:87–98.
[76] Tao R, Li X, Yudhanto A, Alfano M, Lubineau G. Laser-based interfacial patterning enables toughening of CFRP/epoxy joints through bridging of adhesive ligaments. Composites A 2020;139:106094. http://dx.doi.org/10.1016/j.compositesa.2020.106094.
[77] Turon A, Camanho P, Costa J, Dávila C. A damage model for the simulation of delamination in advanced composites under variable-mode loading. Mech Mater 2006;38(11):1072–89. http://dx.doi.org/10.1016/j.mechmat.2005.10.003.
[78] Lindgaard E, Bak B, Glud J, Sjølund J, Christensen E. A user programmed cohesive zone finite element for ANSYS Mechanical. Eng Fract Mech 2017;180:229–39.
[79] Trabal GG, Bak BLV, Chen B, Lindgaard E. An adaptive floating node based formulation for the analysis of multiple delaminations under quasi-static loading. Composites A 2022;106846. http://dx.doi.org/10.1016/j.compositesa.2022.106846.
[80] Turon A, Camanho P, Costa J, Renart J. Accurate simulation of delamination growth under mixed-mode loading using cohesive elements: Definition of interlaminar strengths and elastic stiffness. Compos Struct 2010;92(8):1857–64. http://dx.doi.org/10.1016/j.compstruct.2010.01.012.
[81] Juntti M, Asp LE, Olsson R. Assessment of evaluation methods for the mixed-mode bending test. J Compos Technol Res 1999;21(1):37–48.
[82] Turon A, Costa J, Camanho P, Dávila C. Simulation of delamination in composites under high-cycle fatigue. Composites A 2007;38(11):2270–82. http://dx.doi.org/10.1016/j.compositesa.2006.11.009, CompTest 2006.
[83] Bak BLV, Turon A, Lindgaard E, Lund E. A simulation method for high-cycle fatigue-driven delamination using a cohesive zone model. Int J Numer Methods Eng 2015;106(3):163–91. http://dx.doi.org/10.1002/nme.5117.

[84] Turon A, Bak B, Lindgaard E, Sarrado C, Lund E. Interface elements for fatigue-driven delaminations in advanced composite materials. In: Camanho PP, Hallett SR, editors. Numerical modelling of failure in advanced composite materials. Woodhead publishing series in composites science and engineering, Woodhead Publishing; 2015, p. 73–91. http://dx.doi.org/10.1016/B978-0-08-100332-9.00003-7.

[85] Carreras L, Turon A, Bak BL, Lindgaard E, Renart J, Martin de la Escalera F, Essa Y. A simulation method for fatigue-driven delamination in layered structures involving non-negligible fracture process zones and arbitrarily shaped crack fronts. Composites A 2019;122(January):107–19. http://dx.doi.org/10.1016/j.compositesa.2019.04.026.

[86] Trabal GG, Bak BLV, Chen B, Carreras L, Lindgaard E. An adaptive floating node based formulation for the analysis of multiple delaminations under high cycle fatigue loading. Composites A 2022;160:107036. http://dx.doi.org/10.1016/j.compositesa.2022.107036.

[87] Carreras L, Bak B, Turon A, Renart J, Lindgaard E. Point-wise evaluation of the growth driving direction for arbitrarily shaped delamination fronts using cohesive elements. Eur J Mech A Solids 2018;72:464–82. http://dx.doi.org/10.1016/j.euromechsol.2018.05.006.